Fracturing and crystal plasticity of garnet under seismic stress in the dry lower continental crust (Musgrave Ranges, Central Australia)

Friedrich Hawemann[1*], Neil Mancktelow[1], Sebastian Wex[1], Giorgio Pennacchioni[2], Alfredo Camacho[3]

1) Department of Earth Sciences, ETH Zurich, CH8092 Zurich, Switzerland
2) Department of Geosciences, University of Padova, Padova, Italy
3) Department of Geological Sciences, University of Manitoba, Winnipeg, Manitoba, R3T 2N2, Canada

* corresponding author friedrich.hawemann@erdw.ethz.ch

Highlights

- garnet deformed by fracturing and crystal-plasticity under dry lower crustal conditions
- Ca-diffusion profiles indicate multiple generations of fracturing
- diffusion is promoted along zones of higher dislocation density
- fracturing indicates transient high-stress (seismic) events in the lower continental crust

Abstract

Garnet is a high strength mineral compared to other common minerals, such as quartz and feldspar, in the felsic crust. In felsic mylonites, garnet typically occurs as porphyroclasts that mostly evade intracrystalline deformation, except under relatively high temperature conditions. The microstructure of garnet in felsic lower-crustal rocks of the Musgrave Ranges (Central Australia) records both fracturing and crystal-plastic deformation. Granulite facies metamorphism at ~ 1200 Ma generally dehydrated the rocks and produced mm-sized garnets in peraluminous gneisses. A later ~ 550 Ma overprint under sub-eclogitic conditions (600-700 °C, 1.1-1.3 GPa) developed mylonitic shear zones and abundant pseudotachylyte, coeval with the neocrystallization of fine-grained, high-calcium garnet. In the mylonites, granulite-facies garnet porphyroclasts have high calcium content along rims and fractures. However, in certain cases, these rims are narrower than equivalent rims along original grain boundaries, indicating contemporaneous diffusion and fracturing of garnet. The fractured garnets exhibit internal crystal-plastic deformation, which coincides with areas of enhanced diffusion, usually along zones of crystal lattice distortion and dislocation walls associated with subgrain rotation recrystallization. Fracturing of garnet under dry lower crustal conditions, in an otherwise viscously flowing matrix, requires transient high differential stress, most likely related to seismic rupture, consistent with the coeval development of abundant pseudotachylyte.

Keywords

Garnet, Fracture, Crystal-Plasticity, Dry Lower Continental Crust, Pseudotachylyte, Seismicity

1 Introduction

A fundamental problem in geology is the limited preservation of processes in the rock record. This is especially the case for transient events, like earthquakes, traces of which are hardly preserved due to later reworking. The best indicators for seismicity in the rock record are pseudotachylytes (Sibson, 1975; Toy et al., 2011), although not every seismic event produces frictional melts and, once formed, ductile creep or later brittle fracturing may erase most traces (Sibson and Toy, 2006; Kirkpatrick and Rowe, 2013).

Garnet is stable in many metamorphic rocks over a large part of the pressure-temperature space, is commonly preserved, and is suitable for a range of geothermobarometers and geochronometers and their combination for geospeedometry (Lasaga, 1983; Caddick et al., 2010; Baxter and Scherer, 2013). Being a high strength mineral (Karato et al., 1995; Wang and Ji, 1999), both brittle and crystal plastic deformation are rarely observed in garnet when compared to the common matrix minerals of the crust, such as quartz and feldspar. However, Dalziel and Bailey (1968) already interpreted elongate garnets in high grade mylonites to be the result of crystal plastic behavior. Advancements since then in electron microscopy, and especially EBSD (electron backscatter diffraction), have allowed detailed investigation of garnet textures (Kunze et al., 1993; Prior et al., 2000, 2002).

Experimental deformation of garnet indicates that differential stresses on the order of a few GPa are required to produce shear fractures and that the onset of crystal plastic behavior for strain rates typical of actively deforming regions (10^{-12} – 10^{-15} s^{-1}; e.g. Behr and Platt, 2011) only occurs at corresponding temperatures of ca. 780 – 640 °C (Wang and Ji, 1999). The observation of fractured garnets in natural samples may therefore be linked to seismic stresses, as suggested by Austrheim et al. (1996), who described fracturing of garnets during

pseudotachylyte formation and fluid-assisted eclogitization of granulites. Trepmann and Stöckhert (2002) also interpreted the microstructure of fractured and offset garnets as evidence for syn-seismic loading and post-seismic creep and, more recently, Austrheim et al. (2017) again associated brittle and crystal-plastic behavior of garnets with lower crustal seismic events. Papa et al. (2018) interpreted similar deep-seated dilatant fracturing of garnet immediately adjacent to pseudotachylyte to be related to thermal shock due to frictional heating rather than to damage associated with propagation of the seismic rupture.

Here we present a study of garnet microstructures from lower crustal rocks of the Musgrave Block in Australia, which:

(1) illustrates the close association between brittle and ductile deformation of garnet under well-established pressure-temperature conditions;
(2) infers deformation mechanisms from the observed microstructure;
(3) explores the close link between deformation and diffusion in garnet;
(4) complements other independent observations indicating transient high stresses in the lower crust.

2 Geological setting

2.1 Regional geology

The Musgrave Block is located in an intraplate position close to the center of the Australian continent (inset Fig. 1). Amalgamation of the different cratonic blocks took place during the Musgravian Orogeny (1120-1200 Ma), which pervasively overprinted ca. 1550 Ma gneisses (Gray, 1978; Camacho and Fanning, 1995). The Petermann Orogeny (~550 Ma) produced a

series of crustal-scale fault zones, most prominently the Woodroffe Thrust and the Mann Fault (Collerson et al., 1972; Major, 1973; Bell, 1978; Camacho and Fanning, 1995; Raimondo et al., 2010; Wex et al., 2017, 2018, 2019). The south-dipping Woodroffe Thrust has a top-to-the-north sense of shear, and juxtaposes the Fregon Subdomain in the south (hanging wall) against the Mulga Park Subdomain in the north (footwall). During the Musgravian Orogeny, the Mulga Park Subdomain attained amphibolite facies conditions while the Fregon Subdomain reached granulite facies (Camacho and Fanning, 1995; Scrimgeour et al., 1999; Scrimgeour and Close, 1999), and depleted the rocks of OH-bearing minerals (Wex et al., 2018; Hawemann et al., 2018).

The Woodroffe Thrust hosts one of the largest occurrences of pseudotachylyte worldwide (Camacho et al., 1995), but all larger scale shear zones in the hanging wall also show abundant pseudotachylyte that developed under lower crustal conditions (Camacho, 1997; Hawemann et al., 2018). Deformation in the Fregon Subdomain associated with the Petermann Orogeny is concentrated along the sub-eclogitic (~650 °C, 1.2 GPa) Davenport Shear Zone and the North Davenport Shear Zone (Fig. 1), with little discernible overprint of the earlier granulites in between (Camacho et al., 1997). The Davenport Shear Zone is a WNW-ESE-striking, strike-slip zone, with a near horizontal stretching lineation. Deformation inside the Davenport Shear Zone itself is heterogeneous and strongly localized (Hawemann et al., 2019).

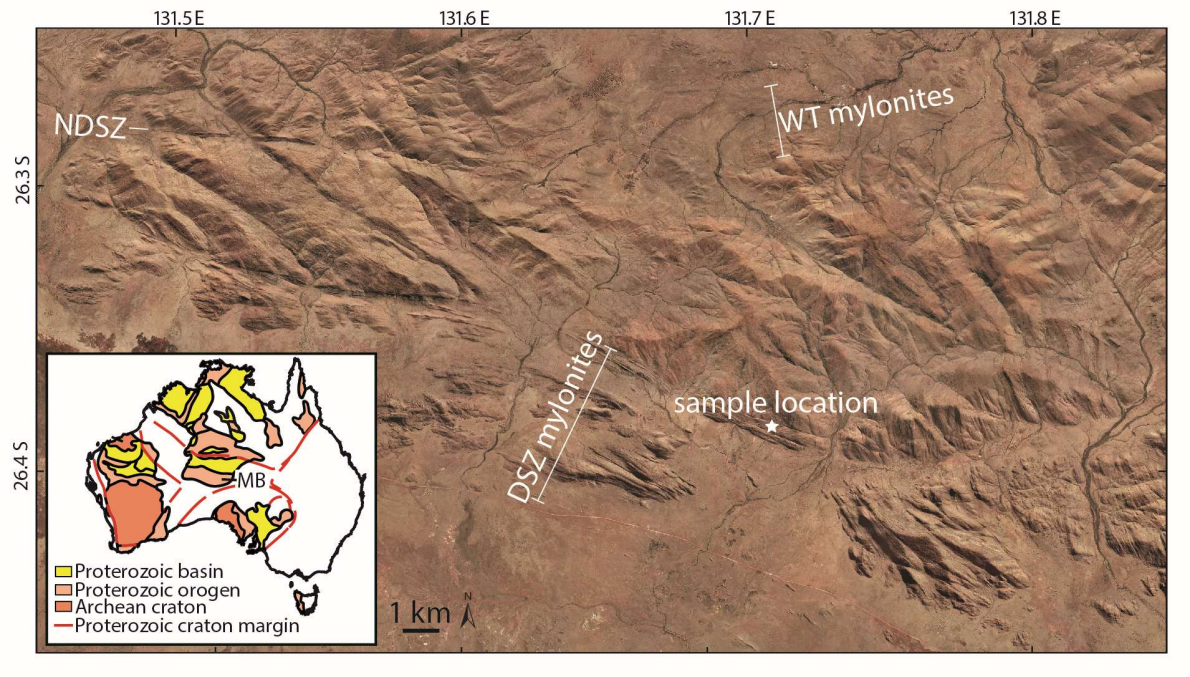

Figure 1: Airborne imagery of the study area with sample location (26.3849 S, 131.7067 E) in the Davenport Shear Zone (DSZ). NDSZ = North Davenport Shear Zone, WT = Woodroffe Thrust. Image from the Department of Primary Industries and Regions, South Australia (PIRSA), 2012. Inset: Location of the Musgrave Block (MB) in between the Australian Cratons. Modified after Evins et al. (2010)

2.2 Sample description

Fractured garnet is ubiquitous in the Fregon Subdomain and is not exclusively found in association with pseudotachylyte veins. However, this study focuses on a representative outcrop for which field relationships, metamorphic, and deformation conditions have been well established (F68, Hawemann et al., 2018; 26.3849 S, 131.7067 E). This outcrop consists of a quartzo-feldspathic mylonite, with millimeter-sized, granulite facies garnets, that includes multiple pseudotachylyte veins and breccias. Pseudotachylytes in the studied outcrop are sheared, as indicated by elongated clasts (Fig. 2a, c), and show the same stretching lineation as the host mylonite. The original discordant relationship to the host foliation is still preserved and cuts perpendicular to the stretching lineation (Fig. 2b).

The syn-mylonitic assemblage associated with the Petermann overprint of felsic granulites is Qz+Kfs+Pl+Gt+Bt+Ky+Ilm+Rt (mineral abbreviations following Whitney and Evans, 2010), and is similar to that of the associated sheared pseudotachylyte (Qz+Kfs+Pl+Gt+Bt+Ky+Rt). The fine-grained garnet growing within the pseudotachylyte gives the rock its caramel-color in macroscopic images (Fig. 2). Fractured garnets are clearly recognizable in polished hand specimens (Fig. 2c) and are very apparent in thin section (Fig. 3). The metamorphic conditions during shearing of this pseudotachylye are estimated at ~600 °C and ~1.1 GPa (Fig. 7 of Hawemann et al., 2018).

Figure 2: Sheared pseudotachylyte in a view orthogonal to the foliation of host felsic mylonite, and perpendicular (a) and parallel (b) to the stretching lineation. c) Polished hand specimen of a sheared pseudotachylyte breccia with the caramel-colored foliated pseudotachylyte matrix including elongated clasts and an elongate fragment of mafic granulite. The host rock shows millimeter-sized garnets with fractures.

3 Garnet microstructure and compositional variation

3.1 Optical microstructure

Granulite facies garnet porphyroclasts in Musgravian peraluminous gneisses mylonitized during the Petermann Orogeny are almost invariably fractured, irrespective of their proximity

to pseudotachylyte (Fig. 3). Large garnet porphyroclasts (>1 mm) are typically slightly elongated with their long axis parallel to the foliation. Fractures in garnets often show offsets in the order of a few 100 µm. It is not possible to determine whether these offsets are primarily due to the initial shear fracture or result from subsequent sliding during ongoing ductile shear. Moreover, no consistent sense of shear can be derived from the offsets (Fig. 3a, b). These discrete fractures are sub-planar, commonly have a consistent orientation at a moderate angle to the foliation, and locally occur in conjugate sets (Fig. 3b). Wide fractures are filled with biotite, kyanite and quartz (Fig. 4b). An apparent late generation of unfilled dilatant fractures is oriented perpendicular to both the foliation and stretching lineation (Fig. 3b). Garnet porphyroclasts commonly contain rutile exsolution lamellae and inclusions of monazite and kyanite (Fig. A1). The latter are present as aggregates with an overall prismatic shape, possibly representing pseudomorphs after sillimanite (Camacho and Fitzgerald, 2010).

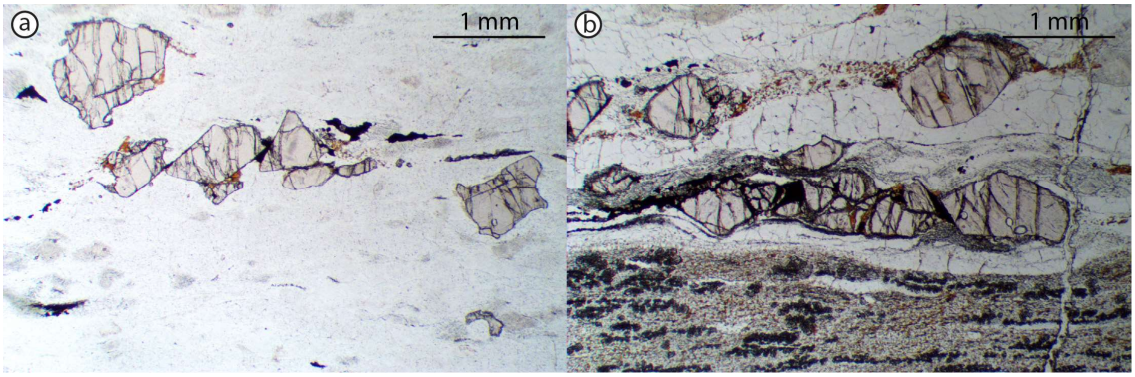

Figure 3: Thin section photomicrographs in plane polarized light of fractured garnets away from pseudotachylyte (a), and close to sheared and recrystallized pseudotachylyte in the lower part of the figure (b). The dark trails of grains elongated in the foliation of the sheared pseudotachylyte are small new garnets.

3.2 Analytical techniques

Quantitative mineral compositions were measured with a JEOL JXA-8200 electron probe micro-analyzer (EPMA), equipped with a tungsten filament, at the Institute of Geochemistry and Petrology at ETH Zurich (Switzerland). Natural standards were used for quantification, and, when available, natural garnet standards were preferred. To reach a spatial resolution of about 1 µm, an acceleration voltage of 10 kV was set (Fig. 8 in Hofer and Brey, 2007). Elemental maps were acquired using energy wavelength-dispersive spectrometers in parallel for calcium, to increase the signal-to-noise ratio. Backscatter electron images (BSE), energy-dispersive spectrometry (EDS) and electron backscatter diffraction (EBSD) mapping was carried out on a Quanta 200F field emission gun (FEG) scanning electron microscope at the ScopeM (Scientific Center for Optical and Electron Microscopy, ETH Zurich). EBSD maps were collected with an acceleration voltage of 20 kV, a sample tilt of 70° and a working distance of 15 mm. Data were post-processed using chemical indexing with the software OIM 7 by EDAX. When necessary, three different clean-up techniques were used: neighbor confidence index correlation, neighbor orientation correlation and grain dilation. Point and map analyses, as well as BSE images, were combined for correlation with optical microscope images in a QGIS-project (Open Source Geospatial foundation). Two lamellae were cut with a focused ion beam (FIB) for transmission electron microscopy (TEM). The microscope used for TEM is a Tecnai F30 with a FEG source operated at 300 kV and equipped with a Gatan 794 MultiScan CCD (ScopeM, ETH Zurich).

3.3 Compostional gradients

Granulite facies garnet has a homogeneous composition of X_{Alm} 0.54, X_{Pyp} 0.40, X_{Grs} 0.03, X_{Sps} 0.03, whereas garnet neocrystallized during the Petermann Orogeny is more Ca-rich (X_{Alm}

0.48, X_{Pyp} 0.28, X_{Grs} 0.22, X_{Sps} 0.02). Grain boundaries of granulite facies garnet and fractures are decorated with a Ca-enriched rim, 20 to 40 µm wide (Fig. 4c). The enrichment is mostly concentric, also affects resorbed areas of the garnet and is therefore most likely the result of diffusion (Camacho et al., 2009). Neocrystallized garnet is present where the grain boundary is in contact with, or close to, plagioclase. The outermost rim of remnant garnet has the same composition as the neocrystallized garnet (Fig. 4d, profile 1). The granulite-facies plagioclase is partially transformed to a more Na-rich plagioclase with needle shaped inclusions of kyanite (bottom of Fig. 4e). This reaction provides Ca for the observed diffusion into garnet (Camacho et al., 2009).

Along fractures across the porphyroclasts, the Ca enrichment is narrower than along the grain boundaries and the grossular component only reaches up to about X_{Grs} 0.1 (Fig. 4d, profile 2). Compositional gradients are also present around inclusions in garnet connected to the outer garnet boundary providing evidence of Ca diffusion along grain boundaries (right part of Fig. 4c, profile 3 in Fig 4d). Profile 4 (Fig. 4d) was measured next to a kyanite inclusion: the diffusion length is still comparable to those of profiles 1-3, but Ca concentrations are much lower. Ca probably diffused along fractures (invisible in the plane of the thin section) towards the inclusion. In summary, the diffusion length at the original grain boundaries is maximized where in contact with plagioclase, and otherwise constant at about 20 µm width. However, variations in diffusion lengths do occur around garnet fragments, without any correlation with the proximity to plagioclase, although the exact relationship in the third dimension is unknown. Surfaces with limited diffusion can often be identified as fracture surfaces, which were exposed to diffusion for a shorter time than original grain boundaries (Fig. 4e). Fractures oriented perpendicular to the foliation and stretching lineation lack any signs of diffusion and are therefore interpreted as later stage dilatant fractures.

Some garnets display more complicated compositional patterns, with zones >100 µm of Ca enrichment extending into the porphyroclast's interior, which are not associated with fractures (e.g. the garnet fragment on the far right in Figure 4e). EBSD-analysis highlights that the three fragments in the right part of Figure 4e most likely originated from the same grain, as they share a common rotation axis (Fig. 4f). The colors in the inverse pole figure map are not solid, reflecting slight variations of orientation within the crystal. Furthermore, the image quality map shows areas of suppressed Kikuchi patterns (grey value) suggestive of higher dislocation density and therefore possible subgrain boundaries (Fig. 4f). The misorientation angle map (Fig. 4g) reveals a complex pattern of varying crystal orientation (all within the order of 5°) in the fragments, with very distributed zones connected to the edges of the crystal, triangular-shaped zones of misorientation (upper left of Fig. 4g), and discrete zones (lower right of Fig. 4g). The discrete zones of misorientation, about 5 µm wide, correlate well with the Ca-enriched zones (compare Fig. 4e, f, garnet fragment on the right).

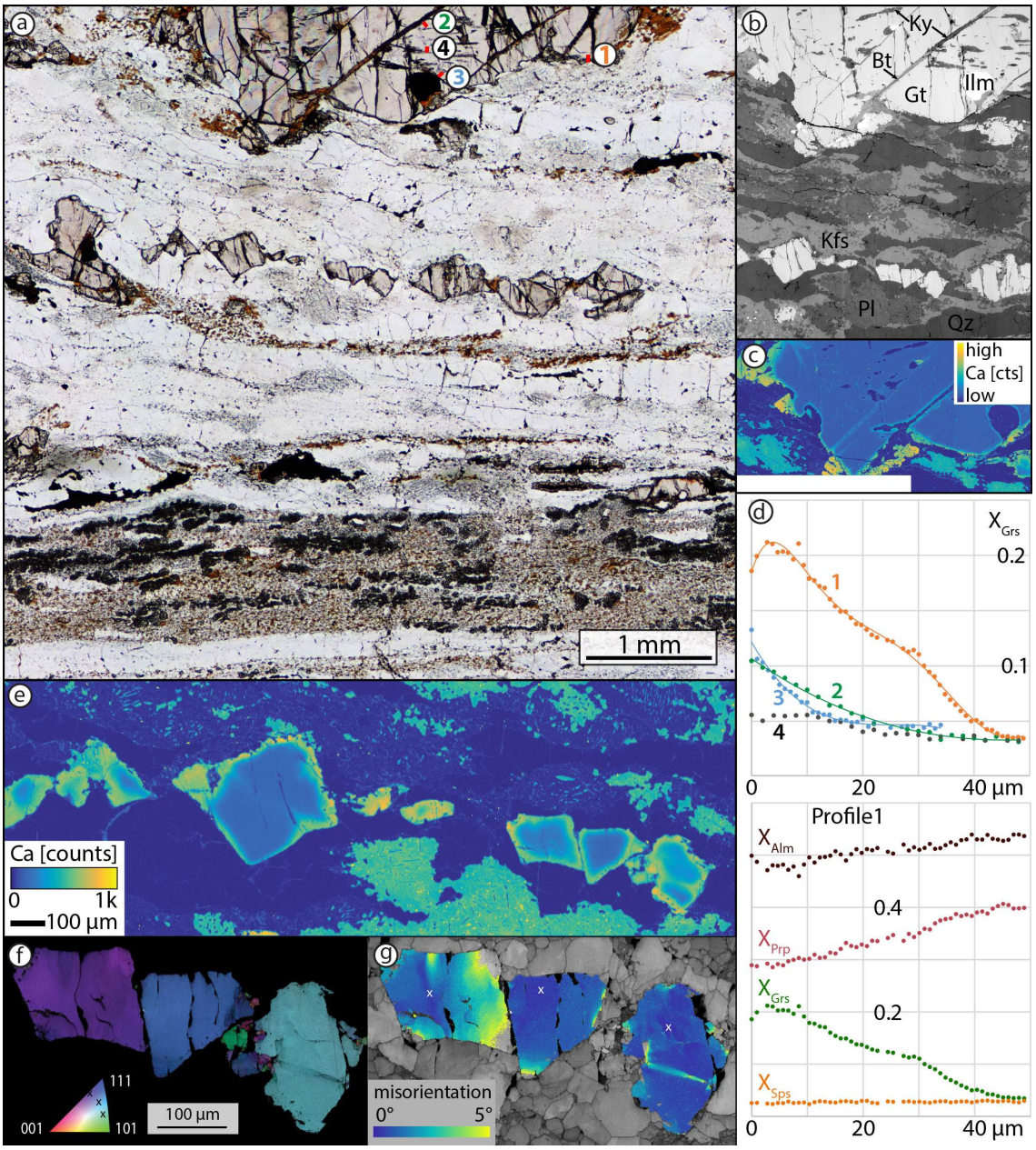

Figure 4: a) Plane polarized light image of thin section with fractured garnets and a pseudotachylyte vein in the lower part of the image. b) BSE image of the upper area of (a), with same scale as (a). c) EPMA X-ray map for Ca reveals the thin diffusion rim along grain boundaries, fractures, and neocrystallized garnet (euhedral, orange). d) Grossular component profiles indicated on (a) (profile lines are not to scale for the sake of visibility); and compositional profiles for four garnet end-members in profile 1. e) EPMA X-ray map for Ca for the garnet fragments in the center of (a). Note the uneven colors in the plagioclase and the blue kyanite needles. f) Inverse pole figure map with superimposed image quality map for garnet fragments shows common rotation pole. g) Misorientation map relative to reference point for each fragment reveals internal lattice distortions.

3.4 Texture of deformed garnets

Two to three orientations of fractures are generally present in a single garnet crystal and coincide with the trace of the (101)-plane derived from EBSD data (Fig. 5a, b). Fracture set (I) in the example of Figure 5a is often associated with a relative rotation of both sides, as visible from the difference in color. In the lower part of the grain, where the fracture density is very high, subgrains are present. The subgrain spatial density increases towards the original grain boundary and some subgrains are "eroded" by ductile shearing and strung out along the foliation. This demonstrates that ductile shearing outlasted subgrain formation and fracturing. Subgrains of less than 10 µm in size formed in the fracture plane (II in Fig. 5a). The fractures described above are all crosscut by dilatant fractures (set III in Fig. 5a), oriented perpendicular to the stretching lineation and foliation, which do not show any associated distortion of the crystal lattice.

The garnet porphyroclast of Figure 5c shows a central fracture as well as a set of two other parallel fractures. The central fracture is the only one with significant offset and is filled with kyanite and quartz. This fracture displays misorientations of more than 5° towards the right-hand side of the scan, but none towards the left-hand side. In the lower left corner of the fragment, subgrains are observed with misorientations, relative to the average orientation, typically in the range of 10°. Misorientation axes are often parallel to (111) and (101). The lowermost fragment shows a wide zone of progressive rotation. The chemical profile in Figure 5e shows the highest Ca counts towards the boundaries of the porphyroclasts and, internally, towards two fractures. The larger fracture with apparent offset of the two garnet fragments exhibits a less well-developed zone of calcium enrichment when compared to the tight fracture with introduced lattice distortion.

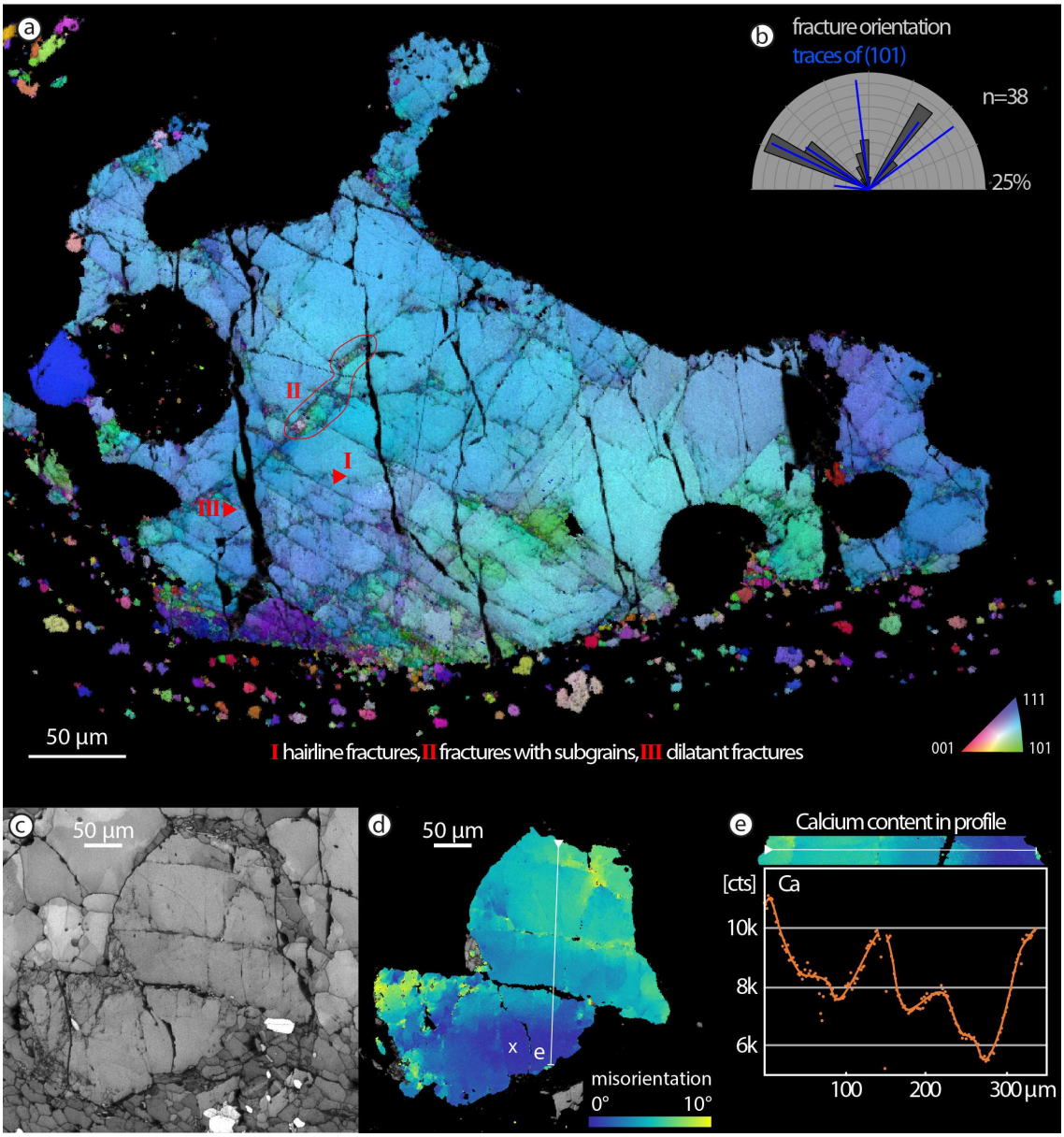

Figure 5: a) Inverse pole figure map of fractured garnet with three dominant orientations of fractures. b) Rose diagram correlating traced fracture orientations and (101)-planes for garnet in (a). c) Image quality map of a fragmented garnet with subgrains. d) Misorientation plot (with respect to the point marked with the white x) shows long wavelength bending in the lower fragment and distortion in the crystal lattice induced by a fracture in the upper fragment. e) EDS-calcium counts for the profile marked as a thin white line in (d).

3.5 TEM investigations

The garnet fragment of Figure 4g was further investigated using TEM, as it includes a narrow zone of misorientation without fractures and is therefore suitable for preparation of FIB-lamellae. As visible in Figure 6a (around profile 1), the image quality map shows a well-defined narrow, darker gray band, possibly indicating high dislocation density. The zone is even more evident in the misorientation plot (Fig. 6b) and changes from about 5 µm wide, with discrete boundaries to the right, to a wider (> 10 µm) band towards the left of the image. In the upper left part of the image, a subgrain boundary with > 5° misorientation transitions into a zone of gradual misorientation. The misorientation axis is consistently parallel to (101) with minor rotation around (111) (Fig. 6c, Fig. A2). Misorientation profiles reveal a slight asymmetry within the narrow band, where the lower boundary appears to be sharper. Misorientation changes more gradually within the wider portion of the misorientation band. Locally, subgrains developed with discrete boundaries, documenting a misorientation of usually around 5-10° (profile 3 in Fig. 6d). The FIB-lamella was cut across the narrow band of misorientations (Fig. 6e). The lower boundary corresponds to a narrow discrete zone, without visible dislocations (Fig. 6f). The upper boundary is marked by a series of dislocation walls and only a few free dislocations are visible, which are often organized in arrays (Fig. 6g, h). The existence of dislocation walls indicates recovery by dislocation climb.

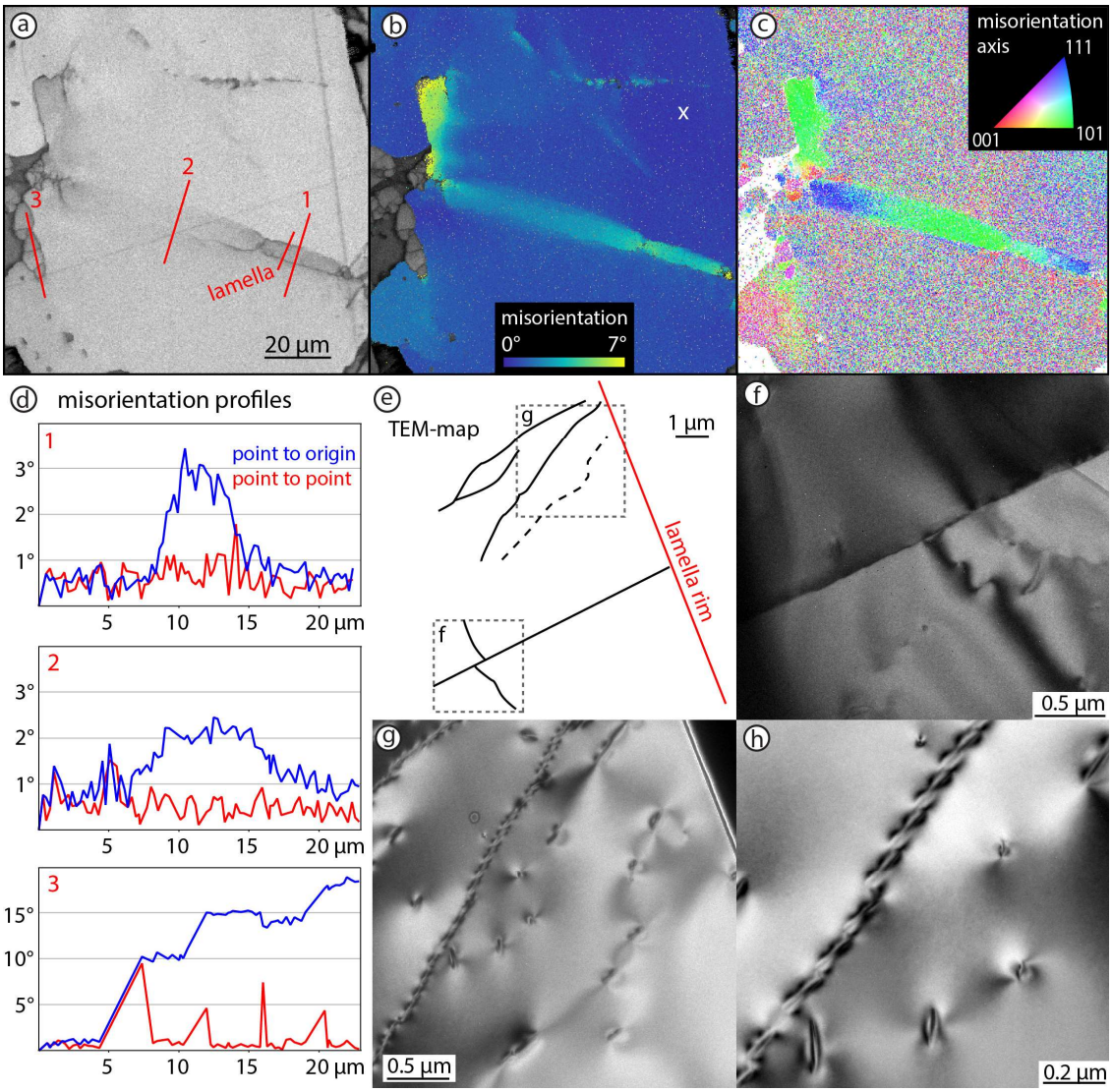

Figure 6: a) Image quality map of the garnet fragment (compare Fig. 4f), with darker zones that can be interpreted as areas of high dislocation density, and location of the FIB-lamella. b) Misorientation plot with respect to the reference point (marked with the white x) shows a discrete zone of misorientation, which has discrete boundaries in the right part of the image, but is more distributed towards the left. c) Misorientation axis plot with respect to the average orientation of the grain shows a consistent rotation around the (101) and (111) axes. For pole figure plots, see Fig. A2. d) Misorientation profiles indicated in a), for (1) the narrow zone, (2) the more distributed zone and (3) for subgrains. e) Overview sketch of the FIB-lamella used for TEM-analysis for correlation with the EBSD data. f) Sharp contrast boundary in the lower part of the lamella. g) Two dislocation walls with a few free dislocations, which are partly linking up parallel to the dislocation walls. h) Detail of the center of (g)

4 Discussion

Garnets in this study show evidence for both brittle and ductile deformation under relatively low temperatures of about 600 °C, as inferred from synchronous diffusion along garnet fractures (Hawemann et al, 2018). This is below the experimentally predicted values for onset of crystal-plastic deformation of garnet (Wang and Ji, 1999) at the higher strain rates considered typical of mylonitic shear zones (> 10^{-14} s^{-1}). In contrast to experiments, many natural examples (Vollbrecht et al., 2006; Bestmann et al., 2008; Austrheim et al., 2017) indicate crystal plasticity of garnet at lower temperatures between 650 °C and 700 °C.

The presence of microstructures and textures consistent with dislocation climb and recovery, as well as subgrain rotation, in garnet at around 600 °C is in agreement with previous studies (Bestmann et al., 2008; Massey et al.,2011). No evidence for grain boundary sliding is observed, since subgrains show rotation around a specific crystallographic axis. Rotation around (111) and (101) is in accordance with the slip systems described by Voegelé et al. (1998).

Multiple generations of overprinting fractures with different orientation demonstrate repeated fracturing events. Tensile fractures do not show any induced lattice distortion or diffusion and therefore occurred after the temperature was too low for diffusion (Camacho et al., 2009), possibly during exhumation (compare Prior, 1993 and Ji et al., 1997).

In contrast to the observations of Austrheim et al. (2017) and Papa et al. (2018) from other examples in the deep continental crust, no “explosive fracturing” or “shattering” of garnet is observed in relict porphyroclasts immediately adjacent to pseudotachylyte. The fractures described here are generally planar and often consistently oriented, in some cases showing single and conjugate shear offsets. Fractured garnet is still present in samples without

pseudotachylyte, where the nearest pseudotachylyte is possibly many meters or more away. Fracturing in this case cannot be related to thermal shock (Papa et al., 2018), but must reflect differential stresses high enough to cause brittle garnet failure.

The narrower Ca diffusion profiles on some fractures relative to garnet rims and crosscutting relationships suggest that fracturing was recurrent under sub-eclogite facies metamorphic conditions, as also indicated by the occasional presence of kyanite in some of some fractures. The presence of kyanite needles and the absence of zoisite/clinozoisite or epidote, as a breakdown product of plagioclase during sub-eclogitic metamorphism (Fig. 3b), indicate relatively dry lower crustal conditions (Hawemann et al., 2018). According to Wayte et al. (1989), this indicates a water activity of < 0.004, calculated for rocks of comparable composition and P-T conditions. However, new biotite did form in dilatant fractures across relict garnet, so conditions were probably not strictly anhydrous. The sheared and recrystallized pseudotachylyte developed a similar synkinematic assemblage as the host mylonite, demonstrating that there is also no marked partitioning of water into the frictional melt, which implies little free or bound water available in the original source rock (e.g. Wex et al., 2018). The effect of pore-fluid pressure on the effective confining pressure must therefore have been negligible.

As reported in Hawemann et al. (2019), the dynamically recrystallized quartz grain size and microstructure in the host rock mylonites indicates that long-term flow stresses were not particularly high, on the order of less than 10 MPa. The ambient pressure of ca. 1.1-1.2 GPa determined for the host rocks should therefore be close to the lithostatic value (Mancktelow, 2008). Figure 7 shows a simple linear plot of the Mohr-Coulomb failure criterion for an angle of internal friction of 30° (coefficient μ = 0.6), a lithostatic load of 1.2 GPa, and no pore fluid

pressure. This plot is only qualitative, since the angle of internal friction could decrease towards higher pressure. However, the summary of experimental results in Byerlee (1978) indicates that there may be little change at least up to pressures similar to those considered here. It follows that the differential stress for fracture initiation must have been of the same order as the confining pressure (Fig. 7). As discussed in detail in Hawemann et al. (2019), such high differential stresses, leading to garnet fracture and the development of abundant pseudotachylyte, can only have been transient and presumably related to repeated short-term seismic events in the lower continental crust (Hawemann et al., 2018; Jamtveit et al, 2018; Menegon et al., 2017). The lack of shattered garnet adjacent to pseudotachylyte in these samples may reflect drier conditions relative to those in the Bergen Arc (Austrheim et al., 2017) and Mont Mary (Papa et al., 2018). The samples studied could therefore represent one end-member of the lower continental crust, where deformation occurs without the initial presence or influx of free water during fracturing and subsequent crystal-plastic deformation.

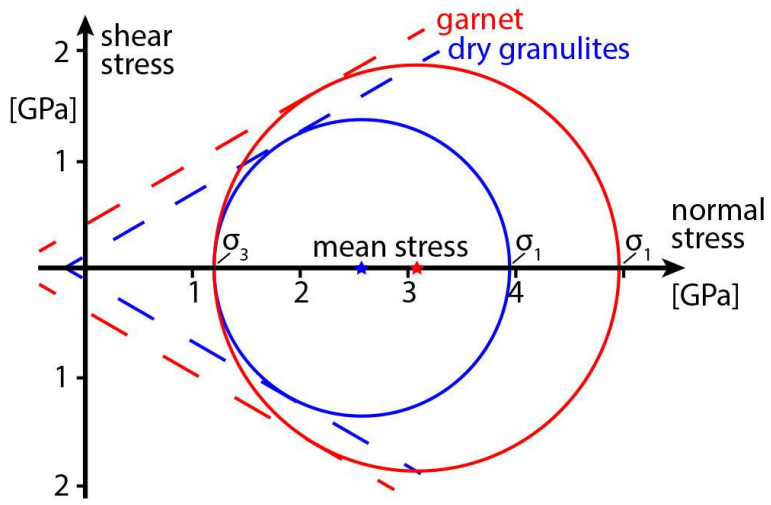

Figure 7: Mohr circles for fracturing of dry granulites and garnet at 1.2 GPa lithostatic load

5 Conclusions

In dry lower continental crust deformed under conditions of ca. 600 °C and 1.1 GPa, garnet shows both single and conjugate sets of shear fractures, fractures with associated subgrains and induced lattice damage around fractures, subgrain formation without fracturing, and late-stage dilatant fractures. Most of these fractures show a strong crystallographic control, with fracturing preferentially occurring along the (101) planes of garnet. Dynamic recrystallization is evident from inferred subgrain rotation recrystallization and recovery is manifested by the presence of dislocation walls. The observed microstructures of garnets are interpreted to record transient high stresses during deep seismic events in the lower crustal Fregon Subdomain. This is also indicated by the abundant occurrence of pseudotachylyte developed under similar lower crustal conditions and, possibly, by the variability of recrystallized quartz grain sizes including values down to a few micrometers (Hawemann et al. 2009b). The studied example represents one end-member of lower continental crustal behavior where, because of earlier metamorphic dehydration and the intracratonic position well removed from the plate margin, rocks were initially dry and water was not introduced during fracturing and crystal-plastic deformation.

Acknowledgements

We gratefully acknowledge permission granted to work on the Anangu Pitjantjatjara Yankunytjatjara Lands (APY) to carry out our field work in the area. The Northern Territory Geological Survey (NTGS) and Basil Tikoff (Department of Geoscience, University of Wisconsin) are thanked for their logistical support and the Nicolle family of Mulga Park station for their hospitality. The Scientific Center for Optical and Electron Microscopy (ScopeM) provided the facilities for the scanning electron microscopy work, and help by Karsten Kunze,

Luiz Morales and Fabian Gramm is especially acknowledged. Luca Menegon is thanked for his review of the first author's doctoral thesis. This project was financed by the Swiss National Science Foundation (SNF) grant 200021_146745 and by the University of Padova (BIRD175145/17: The geological record of deep earthquakes: the association pseudotachylyte-mylonite).

References

Austrheim, H., Dunkel, K.G., Plümper, O., Ildefonse, B., Liu, Y., Jamtveit, B., 2017. Fragmentation of wall rock garnets during deep crustal earthquakes. Science Advances 3, e1602067. https://doi.org/10.1126/sciadv.1602067

Austrheim, H., Erambert, M., Boundy, T.M., 1996. Garnets recording deep crustal earthquakes. Earth and Planetary Science Letters 139, 223–238. https://doi.org/10.1016/0012-821X(95)00232-2

Baxter, E.F., Scherer, E.E., 2013. Garnet Geochronology: Timekeeper of Tectonometamorphic Processes. Elements 9, 433–438. https://doi.org/10.2113/gselements.9.6.433

Bell, T.H., 1978. Progressive deformation and reorientation of fold axes in a ductile mylonite zone: the Woodroffe thrust. Tectonophysics 44, 285–320.

Behr, W.M., Platt, J.P., 2011. A naturally constrained stress profile through the middle crust in an extensional terrane. Earth and Planetary Science Letters 303, 181-192.

Bestmann, M., Habler, G., Heidelbach, F., Thöni, M., 2008. Dynamic recrystallization of garnet and related diffusion processes. Journal of Structural Geology 30, 777–790. https://doi.org/10.1016/j.jsg.2008.02.007

Caddick, M.J., Konopasek, J., Thompson, A.B., 2010. Preservation of Garnet Growth Zoning and the Duration of Prograde Metamorphism. Journal of Petrology 51, 2327–2347. https://doi.org/10.1093/petrology/egq059

Camacho, A., Compston, W., McCulloch, M., McDougall, I., 1997. Timing and exhumation of eclogite facies shear zones, Musgrave Block, central Australia. Journal of Metamorphic Geology 15, 735–751.

Camacho, A., Fanning, C.M., 1995. Some isotopic constraints on the evolution of the granulite and upper amphibolite facies terranes in the eastern Musgrave Block, central Australia. Precambrian Research 71, 155–181.

Camacho, A., Fitz Gerald, J.D., 2010. Misidentification of oxide phases and of twinned kyanite: implications for inferred P-T histories of the Musgrave Block, central Australia. Journal of the Virtual Explorer 35. https://doi.org/10.3809/jvirtex.2011.00275

Camacho, A., Vernon, R.H., Fitz Gerald, J.D., 1995. Large volumes of anhydrous pseudotachylyte in the Woodroffe Thrust, eastern Musgrave Ranges, Australia. Journal of Structural Geology 17, 371–383.

Camacho, A., Yang, P., Frederiksen, A., 2009. Constraints from diffusion profiles on the duration of high-strain deformation in thickened crust. Geology 37, 755–758.

Collerson, K.D., Oliver, R.L., Rutland, R.W.R., 1972. An example of structural and metamorphic relationships in the Musgrave orogenic belt, central Australia. Journal of the Geological Society of Australia 18, 379–393. https://doi.org/10.1080/00167617208728776

Dalziel, I.W.D., Bailey, S.W., 1968. Deformed garnets in a mylonitic rock from the Grenville Front and their tectonic significance. American Journal of Science 266, 542–562. https://doi.org/10.2475/ajs.266.7.542

Evins, P.M., Smithies, R.H., Howard, H.M., Kirkland, C.L., Wingate, M.T.D., Bodorkos, S., 2010. Redefining the Giles Event within the setting of the 1120-1020 Ma Ngaanyatjarra Rift, West Musgrave Province, Central Australia. Geological Society of Western Australia, East Perth, W.A.

Gray, C.M., 1978. Geochronology of granulite - facies gneisses in the western Musgrave Block, Central Australia. Journal of the Geological Society of Australia 25, 403–414. https://doi.org/10.1080/00167617808729050

Hawemann, F., Mancktelow, N.S., Wex, S., Camacho, A., Pennacchioni, G., 2018. Pseudotachylyte as field evidence for lower-crustal earthquakes during the intracontinental Petermann Orogeny (Musgrave Block, Central Australia). Solid Earth 9, 629–648. https://doi.org/10.5194/se-9-629-2018

Hawemann, F., Mancktelow, N.S., Pennacchioni, G., Wex, S., Camacho, A., 2019. Weak and slow, strong and fast: How shear zones evolve in a dry continental crust (Musgrave Ranges, Central Australia). Journal of Geophysical Research: Solid Earth. https://doi.org/10.1029/2018JB016559

Hofer, H.E., Brey, G.P., 2007. The iron oxidation state of garnet by electron microprobe: Its determination with the flank method combined with major-element analysis. American Mineralogist 92, 873–885. https://doi.org/10.2138/am.2007.2390

Jamtveit, B., Ben-Zion, Y., Renard, F., Austrheim, H., 2018. Earthquake-induced transformation of the lower crust. Nature 556, 487-491.

Ji, S., Zhao, P., Saruwatari, K., 1997. Fracturing of garnet crystals in anisotropic metamorphic rocks during uplift. Journal of Structural Geology 19, 603–620.

Karato, S., Wang, Z., Liu, B., Fujino, K., 1995. Plastic deformation of garnets: systematics and implications for the rheology of the mantle transition zone. Earth and Planetary Science Letters 130, 13–30.

Kirkpatrick, J.D., Rowe, C.D., 2013. Disappearing ink: How pseudotachylytes are lost from the rock record. Journal of Structural Geology 52, 183–198. https://doi.org/10.1016/j.jsg.2013.03.003

Kunze, K., Wright, S.I., Adams, B.L., Dingley, D.J., 1993. Advances in automatic EBSP single orientation measurements. Texture, Stress, and Microstructure 20, 41–54.

Lasaga, A.C., 1983. Geospeedometry: an extension of geothermometry, in: Kinetics and Equilibrium in Mineral Reactions. Springer, pp. 81–114.

Major, R. B. (1973). Explanatory Notes for the Woodroffe 1: 250 000 Geological Map SG/52-12 (1st ed.). Adelaide, Australia: Geological Survey of South Australia.

Massey, M.A., Prior, D.J., Moecher, D.P., 2011. Microstructure and crystallographic preferred orientation of polycrystalline microgarnet aggregates developed during progressive creep,

recovery, and grain boundary sliding. Journal of Structural Geology 33, 713–730. https://doi.org/10.1016/j.jsg.2010.12.009

Menegon, L., Pennacchioni, G., Malaspina, N., Harris, K., & Wood, E., 2017. Earthquakes as precursors of ductile shear zones in the dry and strong lower crust. Geochemistry, Geophysics, Geosystems, 18. https://doi. org/10.1002/2017GC007189

Papa, S., Pennacchioni, G., Angel, R.J., Faccenda, M., 2018. The fate of garnet during (deep-seated) coseismic frictional heating: The role of thermal shock. Geology 46, 471–474. https://doi.org/10.1130/G40077.1

Prior, D.J., 1993. Sub-critical fracture and associated retrogression of garnet during mylonitic deformation. Contributions to Mineralogy and Petrology 113, 545–556. https://doi.org/10.1007/BF00698322

Prior, D.J., Wheeler, J., Brenker, F.E., Harte, B., Matthews, M., 2000. Crystal plasticity of natural garnet: New microstructural evidence. Geology 28, 1003. https://doi.org/10.1130/0091-7613(2000)28<1003:CPONGN>2.0.CO;2

Prior, D.J., Wheeler, J., Peruzzo, L., Spiess, R., Storey, C., 2002. Some garnet microstructures: an illustration of the potential of orientation maps and misorientation analysis in microstructural studies. Journal of Structural Geology, Microstructural Processes: A Special Issue in Honor of the Career Contributions of R.H. Vernon 24, 999–1011. https://doi.org/10.1016/S0191-8141(01)00087-6

Raimondo, T., Collins, A.S., Hand, M., Walker-Hallam, A., Smithies, R.H., Evins, P.M., Howard, H.M., 2010. The anatomy of a deep intracontinental orogen. Tectonics 29, n/a-n/a. https://doi.org/10.1029/2009TC002504

Sibson, R.H., 1975. Generation of pseudotachylyte by ancient seismic faulting. Geophysical Journal International 43, 775–794.

Sibson, R.H., Toy, V.G., 2006. The habitat of fault-generated pseudotachylyte: Presence vs. absence of friction-melt, in: Abercrombie, R., McGarr, A., Kanamori, H., Di Toro, G. (Eds.), Geophysical Monograph Series. American Geophysical Union, Washington, D. C., pp. 153–166.

Toy, V.G., Ritchie, S., Sibson, R.H., 2011. Diverse habitats of pseudotachylytes in the Alpine Fault Zone and relationships to current seismicity. Geological Society, London, Special Publications 359, 115–133. https://doi.org/10.1144/SP359.7

Trepmann, C.A., Stöckhert, B., 2002. Cataclastic deformation of garnet: a record of synseismic loading and postseismic creep. Journal of Structural Geology 24, 1845–1856. https://doi.org/10.1016/S0191-8141(02)00004-4

Voegelé, V., Cordier, P., Sautter, V., Sharp, T.G., Lardeaux, J.M., Marques, F.O., 1998. Plastic deformation of silicate garnets. Physics of the Earth and Planetary Interiors 108, 319–338. https://doi.org/10.1016/S0031-9201(98)00111-3

Vollbrecht, A., Pawlowski, J., Leiss, B., Heinrichs, T., Seidel, M., Kronz, A., 2006. Ductile deformation of garnet in mylonitic gneisses from the Münchberg Massif (Germany). Tectonophysics 427, 153–170. https://doi.org/10.1016/j.tecto.2006.05.024

Wang, Z., Ji, S., 1999. Deformation of silicate garnets; brittle-ductile transition and its geological implications. The Canadian Mineralogist 37, 525.

Wayte, G.J., Worden, R.H., Rubie, D.C., Droop, G.T.R., 1989. A TEM study of disequilibrium plagioclase breakdown at high pressure: the role of infiltrating fluid. Contributions to Mineralogy and Petrology 101, 426–437. https://doi.org/10.1007/BF00372216

Wex, S., Mancktelow, N.S., Camacho, A., Pennacchioni, G., 2019. Interplay between seismic fracture and aseismic creep in the Woodroffe Thrust, central Australia – Inferences for the rheology of relatively dry continental mid-crustal levels. Tectonophysics 758, 55–72. https://doi.org/10.1016/j.tecto.2018.10.024

Wex, S., Mancktelow, N.S., Hawemann, F., Camacho, A., Pennacchioni, G., 2018. Inverted distribution of ductile deformation in the relatively “dry” middle crust across the Woodroffe Thrust, central Australia. Solid Earth 9, 859–878. https://doi.org/10.5194/se-9-859-2018

Wex, S., Mancktelow, N.S., Hawemann, F., Camacho, A., Pennacchioni, G., 2017. Geometry of a large-scale, low-angle, mid-crustal thrust (Woodroffe Thrust, central Australia): Geometry of a mid-crustal thrust. Tectonics. https://doi.org/10.1002/2017TC004681

Appendix

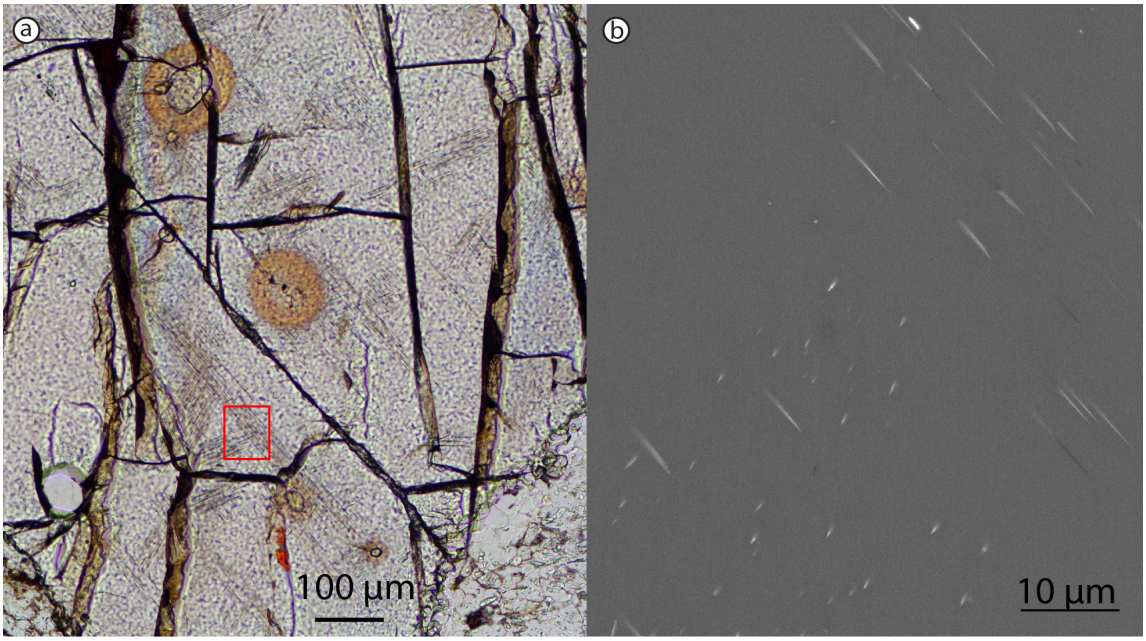

Figure A1: Thin section microphotograph in plane polarized light of a garnet crystal with monazite inclusions (with halos) and rutile-exsolution needles. b) BSE-image of the area indicated with the red box.

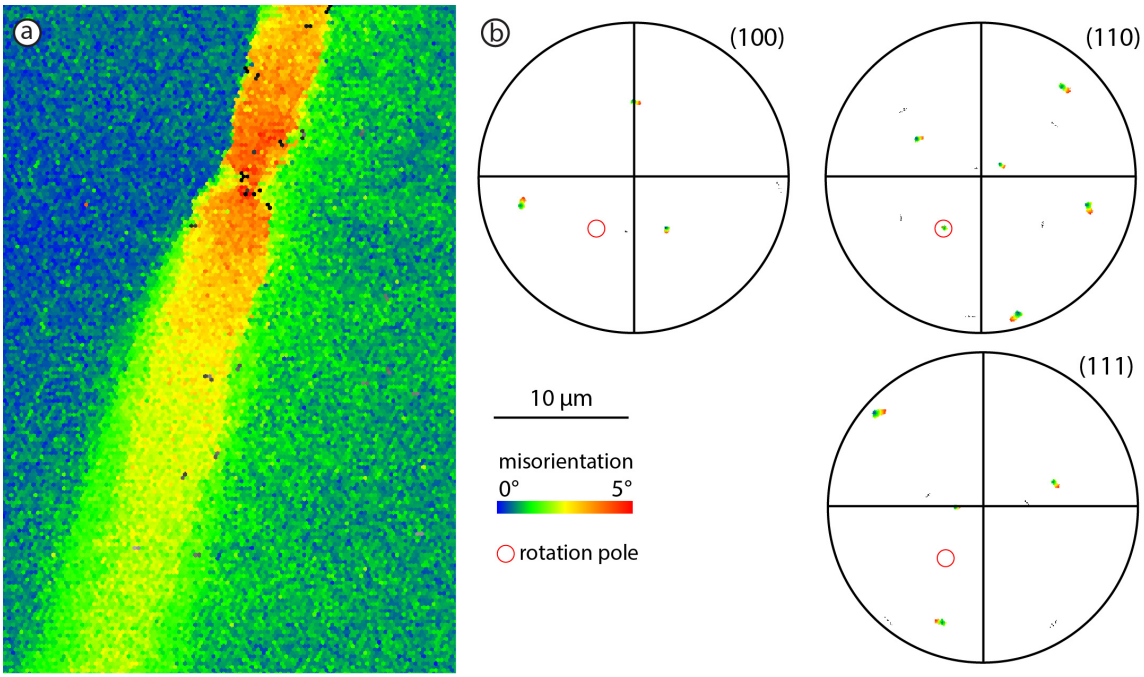

Figure A2: a) Misorientation map-detail for Fig. 6b), with b) pole figure plots for garnet axis with the same color scheme. The plots reveal a rotation around a (101)-axis, as indicated by the red circle.